

# Magnetotransport in HgTe quantum wells with two gate electrodes

© G.M. Minkov<sup>1,2</sup>, O.E. Rut<sup>1</sup>, A.A. Sherstobitov<sup>1,2</sup>, A.V. Germanenko<sup>1</sup>, S.A. Dvoretzki<sup>3</sup>, N.N. Mikhailov<sup>3</sup>

<sup>1</sup> Ural Federal University after the first President of Russia B.N. Yeltsin,  
620062 Yekaterinburg, Russia

<sup>2</sup> M.N. Mikheev Institute of Metal Physics, Ural Branch, Russian Academy of Sciences,  
620108 Yekaterinburg, Russia

<sup>3</sup> Rzhanov Institute of Semiconductor Physics, Siberian Branch, Russian Academy of Sciences,  
630090 Novosibirsk, Russia

E-mail: grigori.minkov@urfu.ru

Received October 8, 2024

Revised October 13, 2024

Accepted October 13, 2024

The magnetotransport properties of HgTe/Hg<sub>1-x</sub>Cd<sub>x</sub>Te quantum wells with a width of 32 and 46 nm in structures with two field electrodes were investigated. The analysis of the Shubnikov-de Haas oscillations, along with the analysis of intersubband magnetooscillations, allowed us to obtain information about the population of the spin branches of the electron spectrum split by spin-orbital interaction due to the asymmetry of the quantum well not only when the electron concentration changes, but also when the symmetry of the quantum well changes at a given electron concentration. The data obtained are interpreted using the results of the calculation of the energy spectrum performed within the framework of a self-consistent approach in a four-band *kP*-model. It is shown that taking into account the complexity of the spectrum of the studied systems is fundamentally important for the interpretation of experimental data.

**Keywords:** HgTe, quantum wells, magnetotransport, Shubnikov-de Haas oscillations.

DOI: 10.61011/SC.2024.08.59890.7175

## 1. Introduction

The specific properties of HgTe/Hg<sub>1-x</sub>Cd<sub>x</sub>Te quantum wells (QWs) stem from the fact that HgTe is a zero-gap semiconductor with an inverted spectrum (band  $\Gamma_6$  is located lower in energy than valence band  $\Gamma_8$ ) and Hg<sub>1-x</sub>Cd<sub>x</sub>Te barriers are semiconductors with a normal band order. This translates into a very strong dependence of the type of energy spectrum in spatial quantization on the QW width ( $d$ ). As  $d$  increases, the spectrum changes from a normal gap one (at  $d < 6.3$  nm) to inverted gap (at  $d > 6.3$  nm) and inverted semi-metallic (at  $d > 14$ – $16$  nm) spectra, eventually transforming into a spectrum of a three-dimensional topological insulator.

As in most two-dimensional semiconductor systems, experimental studies of mercury telluride QWs are performed for structures with a field electrode, which provides an opportunity to alter both the conductivity type (from electron to hole and vice versa) and the concentration of carriers within a fairly wide range by adjusting voltage  $V_g$  applied to this electrode. However,  $V_g$  alters both the carrier concentration and the QW symmetry. Such a change in QW symmetry is not very important for moderately wide QWs ( $d < 20$  nm) that were studied in some detail in a number of papers (see, e.g., [1–6]), and their energy spectrum and transport phenomena are characterized reasonably well within the multiband *kP* model.<sup>1</sup>

Changes in symmetry of wider QWs ( $d > 20$ – $30$  nm) induced by the gate voltage have a significant influence

<sup>1</sup> Certain discrepancies between theoretical calculations and experimental data were discussed in [7].

on the energy spectrum and magnetotransport phenomena. The  $V_g$  variation causes strong spin-orbit splitting of the spectrum and triggers the formation of two single-spin spectrum branches. The ratio of electron concentrations in these branches reaches 2.5–3.0. Shubnikov-de Haas (SdH) oscillations become complex in this case (beating of the oscillation amplitude is observed), and difference frequency  $f_3 = f_1 - f_2$  emerges in the Fourier spectrum alongside with harmonics  $f_1$  and  $f_2$  corresponding to electron concentrations  $n_1$  and  $n_2$  in the branches. This frequency represents magneto-intersubband oscillations (MISO) with their amplitude proportional to the rate of transitions between branches, which, in turn, is set by the overlap of electron wave functions in the branches.

Theory predicts that the electron wave functions in these branches should become more and more strongly localized near the QW walls as the concentration increases; therefore, with increasing total electron concentration  $n = n_1 + n_2$ , the overlap of wave functions (and, consequently, the probability of transitions) decreases. This implies that the ratio of amplitudes of MISO and SdH oscillations should decrease with increasing electron concentration. Thus, the discovery of a directly opposite dependence of this ratio on  $n$  in structures with  $d > 30$  nm was unexpected. Specifically, it was found that this ratio increases by a factor of 4–5 as long as one subband of spatial quantization is populated [8]. To interpret the obtained results, the authors performed a self-consistent calculation of the spectrum, which revealed that the observed increase in the amplitude ratio of MISO and SdH oscillations is the result of repulsion from the QW wall of the wave functions of states localized at the wall

closest to the gate with an increase in  $V_g$ . This effect is a manifestation of negative polarizability of the electron gas in wide HgTe quantum wells [8] and enhances the overlap of wave functions of different branches, raises the probability of transitions between them, and, consequently, contributes to an increase in the MISO amplitude. The results of these calculations are qualitatively consistent with experimental data.

In the present study, the magnetoresistance of HgTe/Hg<sub>1-x</sub>Cd<sub>x</sub>Te structures with a quantum well 32 and 46 nm in width and two field electrodes positioned on opposite sides of the QW was measured and analyzed in order to verify the interpretation proposed in [8] and conduct a more thorough examination of the variation of wave functions both with an increase in the electron concentration and with a change in the QW symmetry.

## 2. Experiment

Samples with two field electrodes (top and back) were fabricated based structures with a HgTe quantum well with  $d = 32$  nm (structure 180824) and 46 nm (structure 180823). Samples prepared from the same structures with a single field electrode have been examined earlier in [8]. These are the structures providing the widest range of total electron concentration from  $1 \cdot 10^{11}$  to  $3.5 \cdot 10^{11}$  cm<sup>-2</sup> with only the states of the main subband of spatial quantization being occupied. The architecture of the studied structures is presented in Figure 1. All measurements were carried out in the DC mode without heating of electrons. Additional measurements revealed that, within the limits of experimental accuracy, the dependences on voltage at the field electrodes had no hysteresis.

## 3. Experimental results and discussion

### 3.1. Role of the top field electrode

Since the results obtained in experiments with two structures are close, we focus on the data for structure 180824 with  $d = 32$  nm in the discussion below. Let us first consider the results at zero voltage at back electrode  $V_{bg} = 0$  V.

The dependences of concentrations of electrons and holes on voltage at the top electrode ( $V_{tg}$ ) are shown in Figure 2. At  $V_{tg} > 1$  V, the Hall coefficient ( $R_H$ ) remains independent of the magnetic field through to  $B = 0.5$  T. This demonstrates that one type of current carriers (electrons) is involved in conduction within this gate voltage range, and their concentration is  $n_H = 1/eR_H$ , where  $e$  is the electron charge.

At  $V_{tg} < 1$  V, the Hall coefficient changes sign (from electron at  $B < 0.15$  T to hole) as the magnetic field intensity increases. This behavior is typical of conduction with two types of carriers of different signs. The electron and hole concentrations in this  $V_{tg}$  region were determined using the model of conduction with two types of carriers through

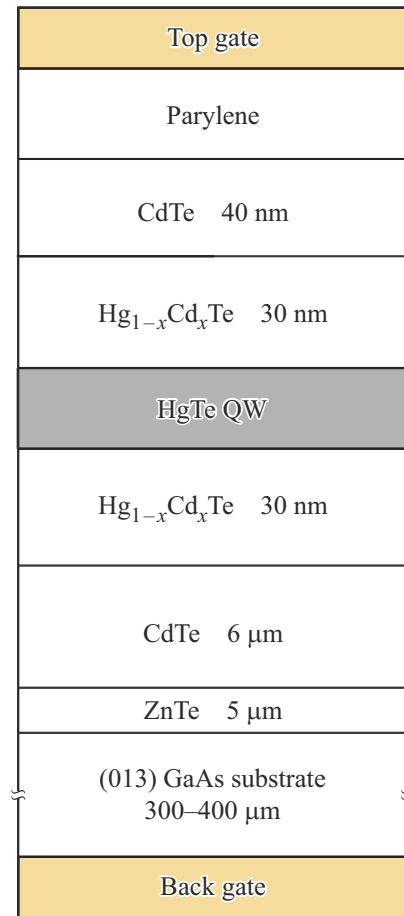


Figure 1. Architecture of the studied structures.

simultaneous fitting of the magnetic-field dependences of  $R_H$  and  $\rho_{xx}$ . In the present study, we limit ourselves to a detailed analysis of magnetotransport in the electron region; therefore, the region where two types of carriers are involved in conduction is given little attention.

The dependence of the concentration of electrons and holes within the entire  $V_{tg}$  range is shown in Figure 2, *a* and reveals that QW charge  $Q/e = n - p$  depends linearly on  $V_{tg}$  as  $Q/e = (0.35 + 1.0 V_{tg}) \cdot 10^{11}$  cm<sup>-2</sup>. This fact and the similarity of derivative  $dQ/dV_{tg}$  to the value determined from capacitance  $C$  between the QW and the top gate demonstrate the lack of parasitic states between the QW and the top gate.

The dependence of mobility of electrons ( $\mu$ ) on their concentration is shown in the inset of Figure 2, *a*. The value of  $\mu$  decreases at concentration  $n > (3.5-4.0) \cdot 10^{11}$  cm<sup>-2</sup> due to the onset of filling of the second subband of spatial quantization [8].

Figure 3 presents oscillations  $\delta\rho_{xx}(B) = \rho_{xx}(B)/\rho_{xx}^{\text{mon}}(B) - 1$ , where  $\rho_{xx}^{\text{mon}}(B)$  is the monotonic component of the  $\rho_{xx}(B)$  dependence, and their Fourier spectra at  $V_{bg} = 0$  and several different  $V_{tg}$  values. It is evident that one component with frequency  $f$  is found in the Fourier spectrum at  $V_{bg} = 1.0$  V. As  $V_{tg}$  grows, it splits into two

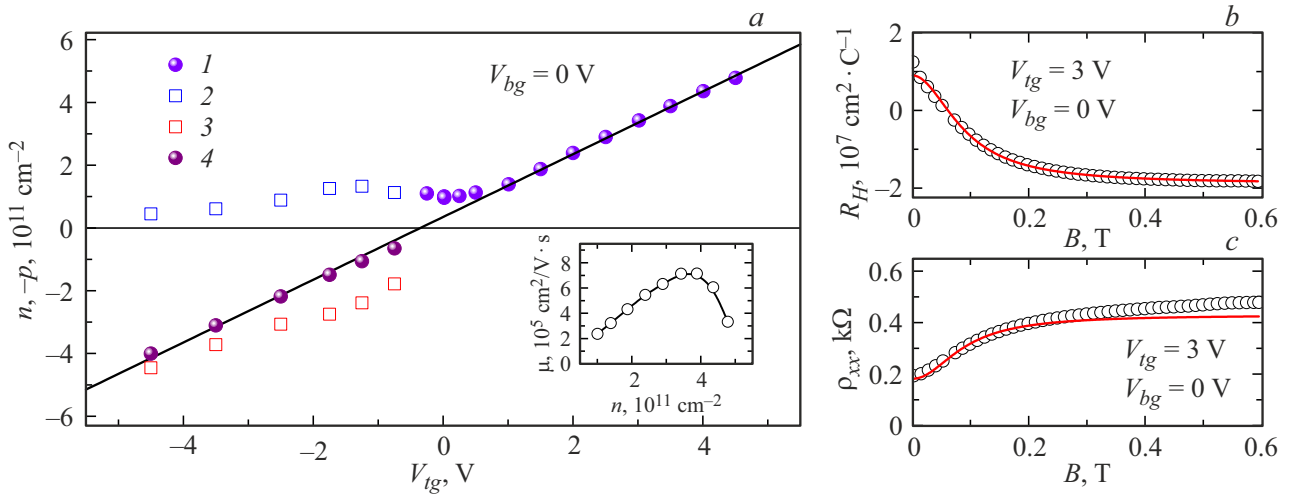


**Figure 2.** (a) Dependences of the concentrations of electrons and holes on voltage at the top field electrode at  $V_{bg} = 0 \text{ V}$  and  $T = 3.8 \text{ K}$ . 1 —  $1/eR_H$  ( $0.3 \text{ T}$ ); 2 and 3 — dependences  $n(V_{tg})$  and  $-p(V_{tg})$ , where electron concentration  $n$  and hole concentration  $p$  were determined through simultaneous fitting of the magnetic-field dependences of  $R_H$  and  $\rho_{xx}$ ; and 4 — dependence of total charge  $Q/e = (n - p)$  in the quantum well on gate voltage. The straight line represents dependence  $(0.35 + 1.0 V_{bg}) \cdot 10^{11} \text{ cm}^{-2}$ . (b) Dependence  $R_H(B)$  at  $V_{tg} = -3 \text{ V}$ . (c) Dependence  $\rho_{xx}(B)$  at  $V_{tg} = -3 \text{ V}$ . Symbols and curves represent the experimental data and the results of fitting, respectively. The inset in Figure 2, a presents the dependence of mobility of electrons determined as  $R_H/\rho_{xx}$  in a  $0.3 \text{ T}$  field on their concentration.

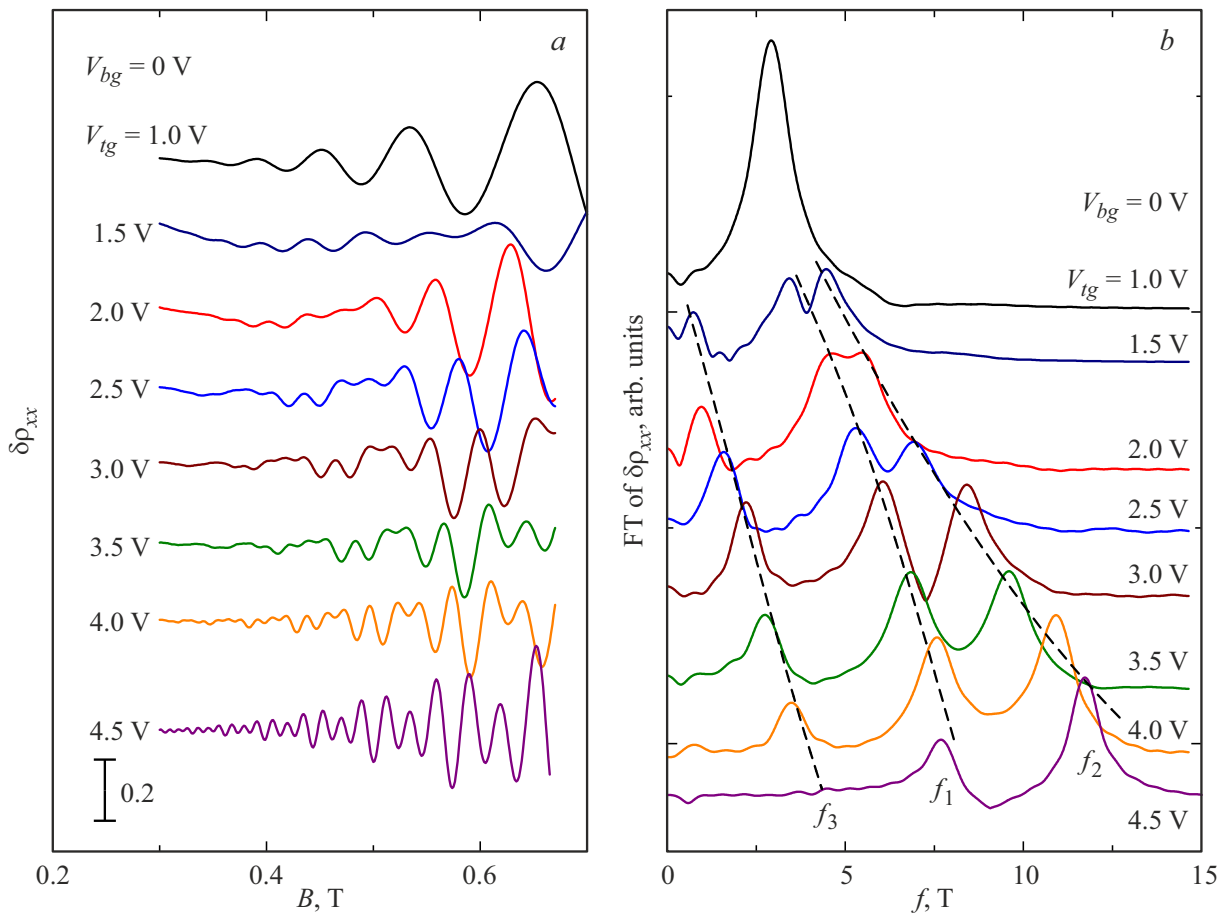


**Figure 3.**  $\delta\rho_{xx}(B)$  oscillations (a) and their Fourier spectra (b) at  $V_{bg} = 0 \text{ V}$  and various  $V_{tg}$  values.  $T = 3.8 \text{ K}$ .

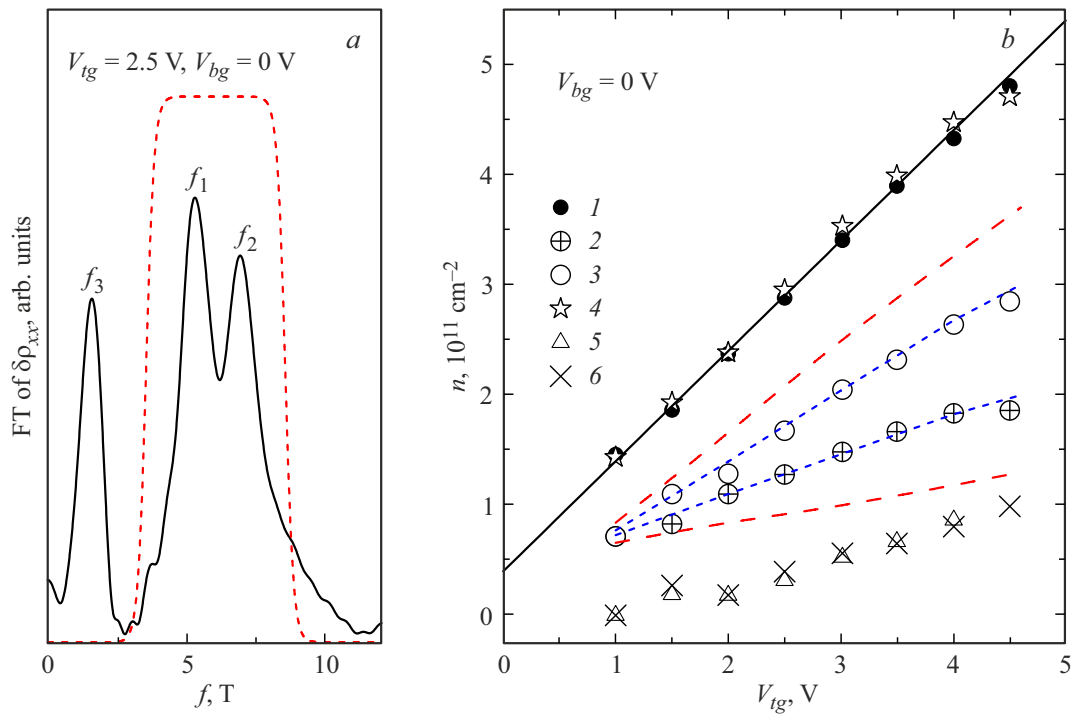


**Figure 4.** (a) Fourier spectrum of oscillations at  $V_{tg} = 2.5$  V and  $V_{bg} = 0$  V. The dotted curve represents the filter used to analyze SdH oscillations. (b) Dependences of electron concentrations on  $V_{tg}$  at  $V_{bg} = 0$  V. 1 —  $1/eR_H$  (0.3 T); 2 and 3 — electron concentrations  $n_1$  and  $n_2$  determined by analyzing SdH oscillations; 4 —  $n_1 + n_2$ ; 5 —  $(e/h)f_3$ ; and 6 —  $n_2 - n_1$ . The solid line represents dependence  $(0.35 + 1.0V_{tg}) \cdot 10^{11} \text{ cm}^{-2}$ . Dashed and dotted lines are the results of self-consistent calculations performed at  $\kappa_{QW} = 20.5$  and  $40.0$ , respectively.

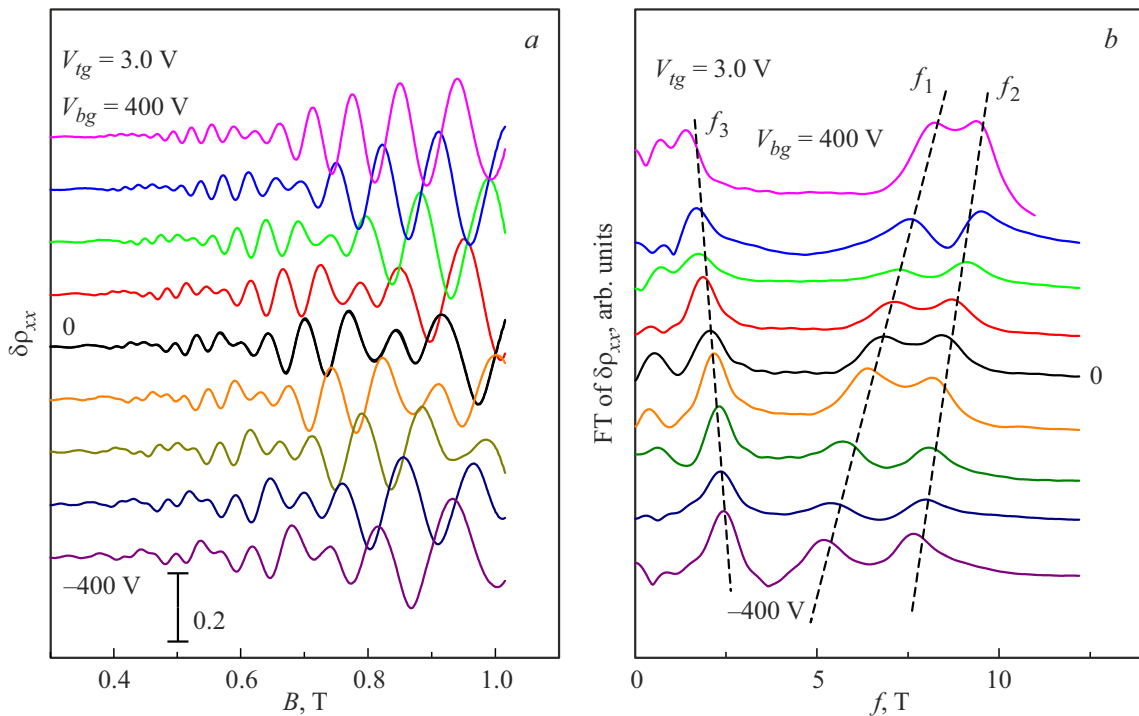


**Figure 5.** (a)  $\delta\rho_{xx}(B)$  oscillations at  $V_{tg} = 3.0$  V with  $V_{bg}$  varying from  $-400$  to  $+400$  V in  $100$  V increments.  $T = 3.5$  K. (b) Fourier spectra of oscillations shown in panel a.

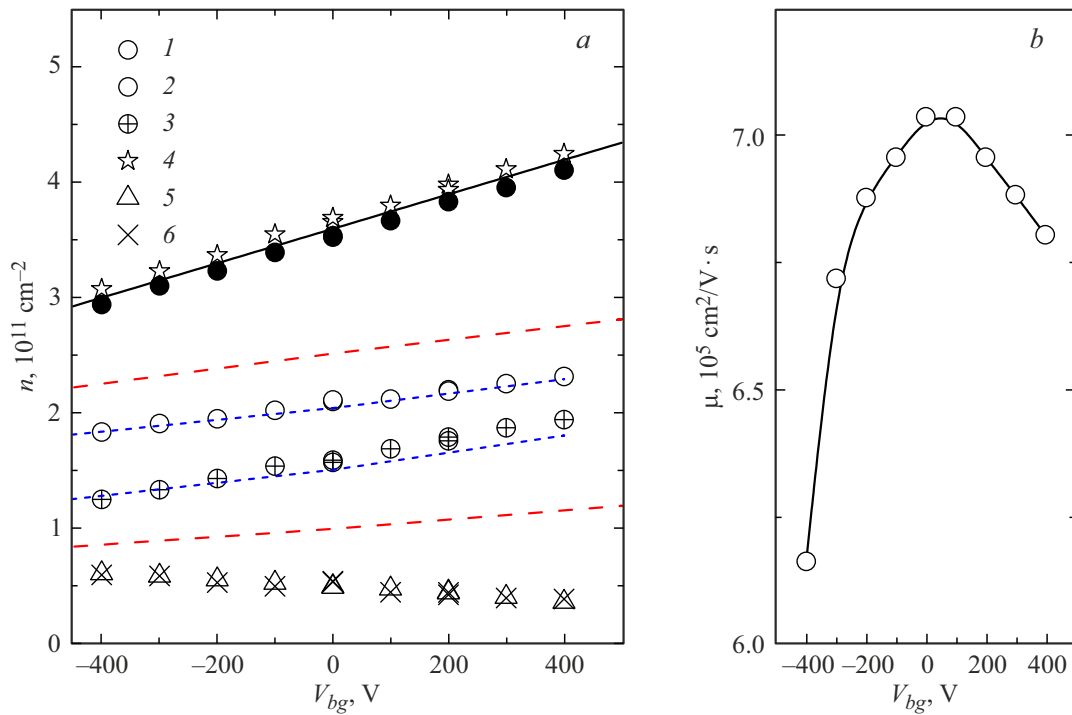


**Figure 6.** (a) Dependences of electron concentrations on  $V_{bg}$  at  $V_{ig} = 3.0$  V. 1 —  $1/eR_H$  (0.3 T); 2 and 3 — electron concentrations  $n_1$  and  $n_2$  determined by analyzing SdH oscillations; 4 —  $n_1 + n_2$ ; 5 —  $(e/h)f_3$ ; and 6 —  $n_2 - n_1$ . The solid line represents dependence  $(3.6 + 0.0015 V_{bg}) \cdot 10^{11} \text{ cm}^{-2}$ . Dashed and dotted lines are the results of self-consistent calculations performed at  $\kappa_{QW} = 20.5$  and  $40.0$ , respectively. (b) Dependence of the electron mobility on  $V_{bg}$  at  $V_{ig} = 3.0$  V.

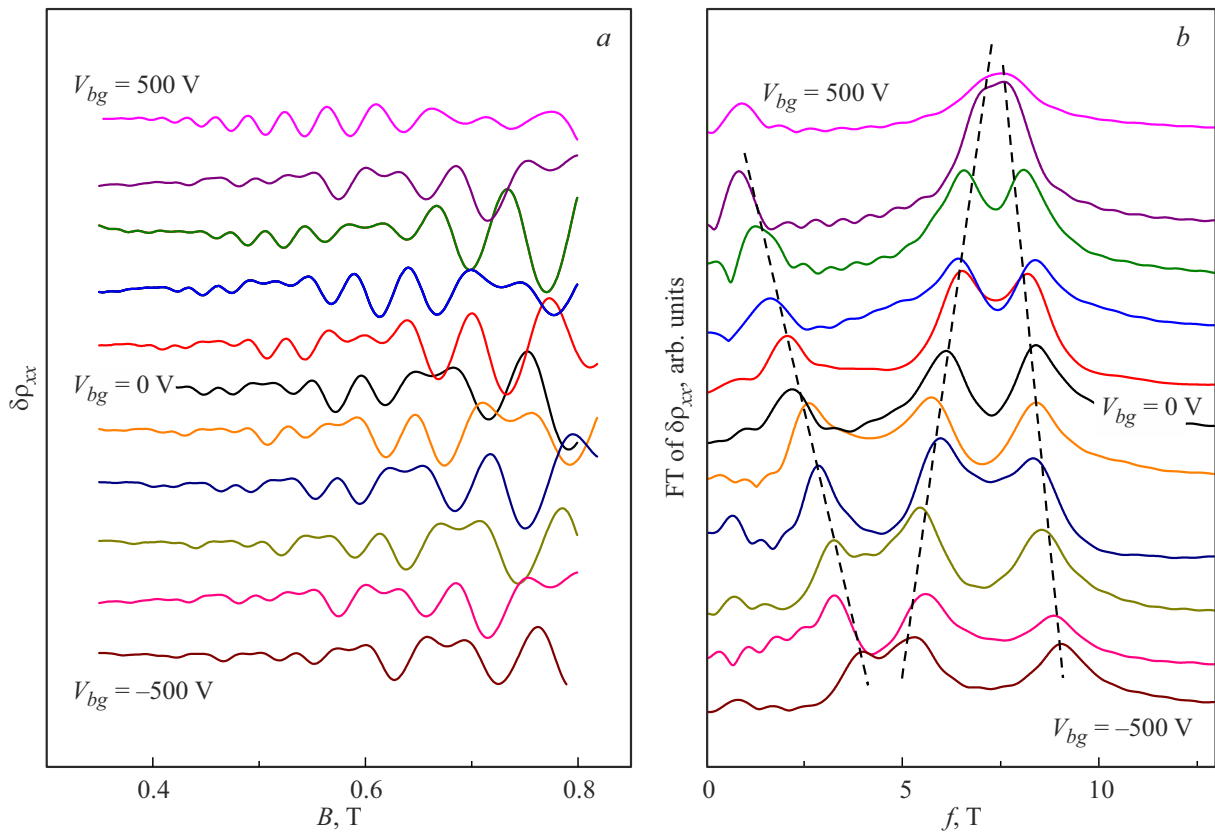


**Figure 7.** (a)  $\delta\rho_{xx}(B)$  oscillations at different  $V_{bg}$  values varying from  $-500$  to  $+500$  V in  $100$  V increments and a  $V_{ig}$  value at which  $n_H = 3.45 \cdot 10^{11} \text{ cm}^{-2}$ . (b) Fourier spectra of oscillations shown in panel a.  $T = 3.5$  K.

components with frequencies  $f_1$  and  $f_2$ , and low-frequency component  $f_3$  emerges. The inverse Fourier transform with a bandpass filter, which is shown in Figure 4, *a* by the dotted curve, was used to determine frequencies  $f_1$  and  $f_2$  more accurately. The resulting curve was characterized by a sum of two oscillating dependences given by the Lifshitz–Kosevich formula [9] (this procedure is detailed in [10]). The concentration determined from frequency  $f$  under the assumption of two-fold degeneracy of Landau levels  $n = 2(e/h)f$  and the sum of concentrations  $n_1 = ef_1/h$  and  $n_2 = ef_2/h$  derived from frequencies  $f_1$  and  $f_2$  under the assumption of one-fold degeneracy of Landau levels match, within the experimental error, the Hall concentration (see Figure 4, *a*). The difference between concentrations determined from frequencies  $f_1$  and  $f_2$  matches the concentration determined based on  $f_3$ . All the above results indicate that (1) at  $V_{tg} \sim 1$  V, the quantum well is near-symmetrical and Landau levels are doubly degenerate; (2) an increase in  $V_{tg}$  leads to violation of the QW symmetry and spin-orbit splitting of the spectrum, and Landau levels become single-spin; and (3) oscillations with frequency  $f_3$  are magneto-intersubband ones. Their amplitude is specified by the rate of transitions between single-spin Landau levels, which, in turn, is determined by the overlap of the wave functions of states split by spin-orbit interaction.

Let us compare the experimental dependences shown in Figure 4, *b* with theoretical ones. A self-consistent approach was used to calculate the electron spectrum and wave functions within the four-band  $kP$  model for this purpose. A self-consistent procedure for solving the Schrödinger and Poisson equations simultaneously was used to introduce the effect of the electric field produced by impurities, electrons, and voltage at the field electrodes.

The dashed lines in Figure 4, *b* represent the result of a self-consistent calculation with the generally accepted values of permittivity in the QW and barriers:  $\kappa(z) = 20.5 - 15.6x(z) + 5.7x^2(z)$ , where  $x(z)$  is the cadmium concentration depending on  $z$ . It is evident that the calculated  $n_1(V_{tg})$  and  $n_2(V_{tg})$  values differ significantly from the experimental ones. This discrepancy for a 32-nm-wide QW was noted in [8]. One possible reason for this is the difference in permittivity between a thin HgTe layer forming the QW and the initial bulk material (see discussion in [11–13]). In addition, the calculation results for QW permittivity  $\kappa_{QW} = 40$  are indicated in Figure 4, *b* by dotted lines. It can be seen that they agree well with the experimental data. Note that the results of similar measurements in QWs with a width ranging from 5 to 46 nm indicate that the experimental and calculated data agree closely at  $\kappa_{QW} = 20.5$  and  $d < 20$  nm; when  $d$  increases,  $\kappa_{QW}$  also needs to be raised (to 70 at  $d = 46$  nm) to achieve a fine fit.

### 3.2. Role of the back field electrode

Let us consider the transformation of oscillations  $\delta\rho_{xx}(B)$  with a change in  $V_{bg}$  at  $V_{tg} = 3.0$  V. The  $\delta\rho_{xx}(B)$  oscillations and their Fourier spectra are shown in Figure 5.

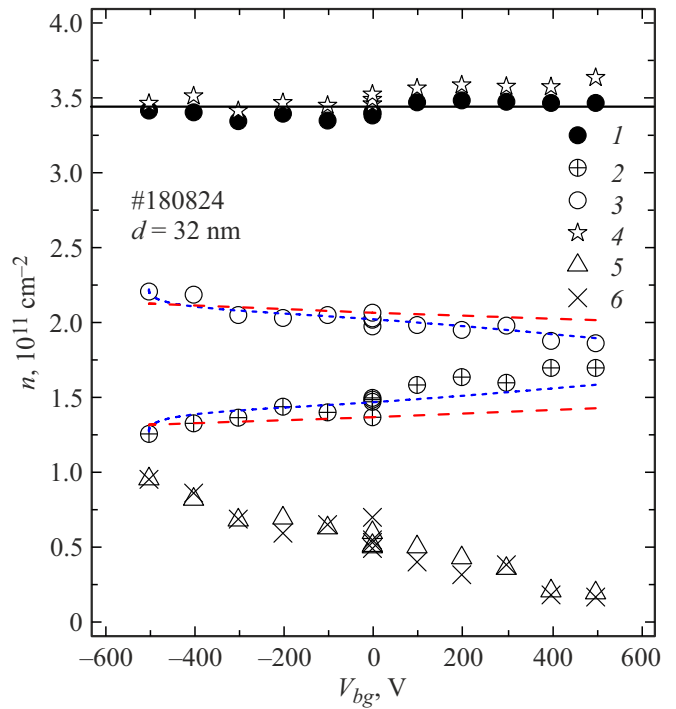


**Figure 8.** Dependences of concentrations  $n_1$  and  $n_2$  on  $V_{bg}$  at  $n_H = 3.45 \cdot 10^{11} \text{ cm}^{-2}$  for structure 180824. 1 —  $1/eR_H$  (0.3 T); 2 and 3 — electron concentrations  $n_1$  and  $n_2$  determined by analyzing SdH oscillations; 4 —  $n_1 + n_2$ ; 5 —  $(e/h)f_3$ ; and 6 —  $n_2 - n_1$ . The solid line corresponds to  $-n_H = 3.45 \cdot 10^{11} \text{ cm}^{-2}$ . Dashed and dotted lines represent results of self-consistent calculations at  $\kappa_{QW} = 20.5$  and  $\kappa_{QW} = 40.0$ , respectively.

The dependences of electron concentration determined from the Hall effect data and the Fourier spectra (Figure 5, *b*) on  $V_{bg}$  are shown in Figure 6, *a*. Figure 6, *b* presents the dependence of mobility, which was determined as  $R_H/\rho_{xx}$  in a 0.3 T field, on  $V_{bg}$ . Within the error limits, this dependence in  $\mu(n_H)$  coordinates matches the dependence shown in the inset of Figure 2, *a*.

It follows from Figure 6, *a* that Hall concentration  $n_H$  matches the sum of concentrations  $n_1$  and  $n_2$  determined by analyzing the Fourier spectra. Voltage  $V_{bg}$  at the back electrode alters the electron concentration in the QW at rate  $dn/dV_{bg} = 0.0015 \text{ cm}^{-2} \cdot \text{V}^{-1}$ . This value is close to the one corresponding to the capacitance per unit area between the back electrode and the quantum well ( $C = \kappa_s \kappa_0 / d_s$ , where  $\kappa_s \kappa_0$  is the substrate permittivity and  $d_s$  is the substrate thickness). Unfortunately, the smallness of this capacitance ( $\sim 0.6$  pF) makes it difficult to measure it experimentally with the required accuracy.

At first glance, the experimental dependences of concentrations on voltage  $V_{tg}$  at the top electrode at  $V_{bg} = 0$  V (Figure 4, *b*) and on voltage  $V_{bg}$  at the back electrode at  $V_{tg} = 3.0$  V (Figure 6, *a*) are natural and understandable. It is also evident from Figure 6, *a* that an increase in concentration due to a change in  $V_{bg}$  leads to a reduction in the concentration difference between the split spectrum branches (i.e., a positive voltage applied to the back

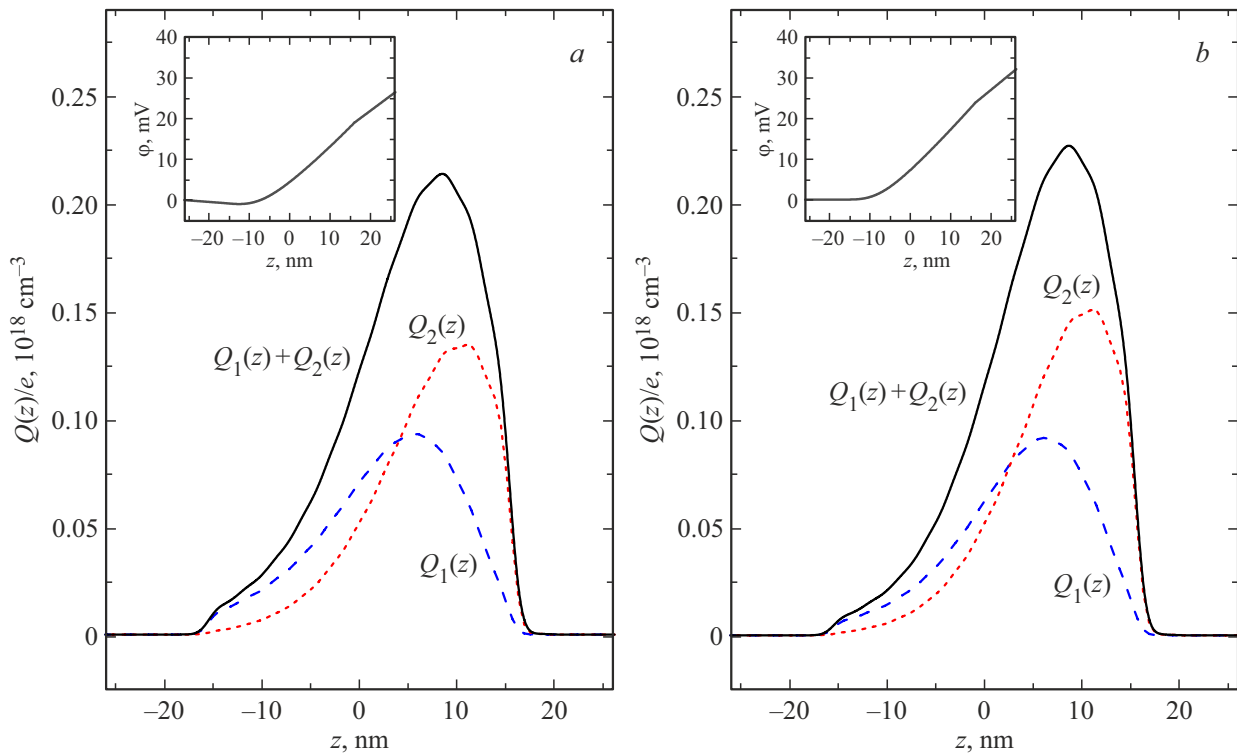


**Figure 9.** Electron density distribution in the  $z$  direction in an asymmetric quantum well with a total electron concentration  $n = 3.45 \cdot 10^{11} \text{ cm}^{-2}$  at (a)  $V_{bg} = 500 \text{ V}$ , when a fraction of charge ( $3.0 \cdot 10^{11} \text{ cm}^{-2}$ ) is induced by the electric field of the top gate and the remaining charge ( $0.45 \cdot 10^{11} \text{ cm}^{-2}$ ) is induced by the field of the back gate, and (b)  $V_{bg} = 0 \text{ V}$ , when all electrons are induced by the top field electrode. Dashed curves represent the contributions of spin branches, and solid curves correspond to the sum of both contributions. The variation of potential  $\phi(z)$  is presented in the inset.

electrode suppresses the QW asymmetry), while an increase in  $V_{ig}$  leads to an enhancement of splitting. However, significant discrepancies are revealed when one compares these results quantitatively with the theoretical ones obtained within the four-band  $kP$  model. The dependences of concentrations in the spectrum branches calculated using QW permittivity  $\kappa_{QW} = 20.5$ , which corresponds to the permittivity of bulk HgTe, are represented in Figures 4, *b* and 6, *a* by dashed lines. A very large discrepancy between the calculated and experimental data is evident. In both cases, an agreement between experiment and theory is achieved only when the QW permittivity is set to  $\kappa_{QW} = 40$ .

### 3.3. Transport under varying quantum well symmetry

The presence of two (top and back) field electrodes allows one to alter the QW symmetry while maintaining a fixed total concentration of electrons. Figure 7, *a* shows the  $\delta\rho_{xx}(B)$  oscillations at a total electron concentration of  $3.45 \cdot 10^{11} \text{ cm}^{-2}$  and different values of voltage at the back field electrode (changing in 100 V increments), while Figure 7, *b* presents the Fourier spectra of these oscillations. These measurements were carried out as follows: at  $V_{bg} = 0 \text{ V}$ ,  $V_{ig} = 3.0 \text{ V}$  was set, which provided a total electron concentration of  $3.45 \cdot 10^{11} \text{ cm}^{-2}$ . Following the

measurement of field dependences of resistance, the voltage at the back field electrode was altered by 100 V, while the voltage at top field electrode was adjusted so that the total concentration remained constant.

The dependences of electron concentrations in the spectrum branches on the value of  $V_{bg}$  obtained by analyzing the Fourier spectra at a fixed total electron concentration of  $3.45 \cdot 10^{11} \text{ cm}^{-2}$  are shown in Figure 8. It is evident that the difference in electron concentration between the spectrum branches increases with negative voltage at the back field electrode, reaching a value of  $\sim 1 \cdot 10^{11} \text{ cm}^{-2}$  ( $\sim 27\%$  of the total electron concentration) at  $V_{bg} = -500 \text{ V}$  and indicating that the quantum well becomes highly asymmetric. When positive gate voltage is raised, the difference in concentration between the branches decreases to  $\sim 0.15 \cdot 10^{11} \text{ cm}^{-2}$  (i.e.,  $< 5\%$ ) at  $V_{bg} = 500 \text{ V}$ , indicating that the well becomes almost symmetrical. This strong suppression of splitting seems counterintuitive, since only a small fraction ( $\sim 0.5 \cdot 10^{11} \text{ cm}^{-2}$ ) of the entire ensemble of electrons in the QW ( $n = 3.45 \cdot 10^{11} \text{ cm}^{-2}$ ) is induced at a voltage of 500 V applied to the back field electrode. However, our intuitive understanding relies on the patterns of electron behavior under spatial confinement in structures with a simple parabolic spectrum, and the present study is focused on HgTe quantum wells.

The dashed and dotted lines in Figure 8 represent the results of a self-consistent calculation within the four-band  $kP$

model with two values of the QW permittivity:  $\kappa_{\text{QW}} = 20.5$  and 40, respectively. Just as in Figures 4, *b* and 6, *a*, a significantly better agreement is found at  $\kappa_{\text{QW}} = 40$ . Note that the best fit for structure 180823 with a quantum well width of 46 nm is achieved at  $\kappa_{\text{QW}} = 70$ . Let us examine the HgTe QW shape and the distribution of electron density determined in calculations. Figure 9 presents the results of self-consistent calculation for  $V_{bg} = 500$  V, when a fraction of charge ( $3.0 \sim 10^{11} \text{ cm}^{-2}$ ) in the QW is induced by the electric field of the top field electrode and the remaining charge ( $0.45 \cdot 10^{11} \text{ cm}^{-2}$ ) is induced by the field of the back field electrode (Figure 9, *a*), and  $V_{bg} = 0$  V, when the entire electron density of  $3.45 \cdot 10^{11} \text{ cm}^{-2}$  in the QW is induced by the electric field of the top electrode (Figure 9, *b*). It is evident that the asymmetry of the electron density distribution and the potential  $\varphi(z)$  variation in these two cases are very close, while the difference in electron concentration between the spin branches varies significantly from  $\sim 0.55 \cdot 10^{11} \text{ cm}^{-2}$  in the first case to  $0.15 \cdot 10^{11} \text{ cm}^{-2}$  in the second case (16 and 3.5% of the total electron concentration of  $3.45 \cdot 10^{11} \text{ cm}^{-2}$ , respectively).

#### 4. Conclusion

Magnetotransport phenomena in mercury telluride quantum wells with a width of 32 and 46 nm in structures with two field electrodes were investigated. Dependences of the electron concentrations in spin branches split by the spin-orbit interaction on the total electron concentration in the quantum well, which is controlled by gate voltages, and on the QW asymmetry at a fixed electron concentration were obtained by analyzing oscillation phenomena. A self-consistent approach for solving the Poisson and Schrödinger equations simultaneously within the four-band *kP* model was used to interpret the obtained data. A quantitative agreement was achieved with the use of generally accepted parameters of the *kP* model, but with a permittivity of the HgTe layer, which forms the quantum well, differing from the permittivity of bulk HgTe:  $\kappa_{\text{QW}} = 40$  and 70 for a QW width of 32 and 46 nm, respectively.

#### Funding

This study was carried out under the state assignment (project FEUZ-2023-0017, research topic „Elektron“ No. 122021000039-4).

#### Conflict of interest

The authors declare that they have no conflict of interest.

#### References

[1] A.M. Shuvaev, G.V. Astakhov, C. Brüne, H. Buhmann, L.W. Molenkamp, A. Pimenov. *Semicond. Sci. Technol.*, **27**, 124004 (2012).

- [2] M.S. Zholudev, A.V. Ikonnikov, F. Teppe, M. Orlita, K.V. Maremyanin, K.E. Spirin, V.I. Gavrilenko, W. Knap, S.A. Dvoretzkiy, N.N. Mikhailov. *Nanoscale Res. Lett.*, **7**, 534 (2012).
- [3] C. Zoth, P. Olbrich, P. Vierling, K.-M. Dantscher, V.V. Bel'kov, M.A. Semina, M.M. Glazov, L.E. Golub, D.A. Kozlov, Z.D. Kvon, N.N. Mikhailov, S.A. Dvoretzkiy, S.D. Ganichev. *Phys. Rev. B*, **90**, 205415 (2014).
- [4] D.A. Kozlov, Z.D. Kvon, E.B. Olshanetsky, N.N. Mikhailov, S.A. Dvoretzkiy, D. Weiss. *Phys. Rev. Lett.*, **112**, 196801 (2014).
- [5] G.M. Minkov, A.V. Germanenko, O.E. Rut, A.A. Sherstobitov, S.A. Dvoretzkiy, N.N. Mikhailov. *Phys. Rev. B*, **89**, 165311 (2014).
- [6] K.-M. Dantscher, D.A. Kozlov, P. Olbrich, C. Zoth, P. Faltermeyer, M. Lindner, G.V. Budkin, S.A. Tarasenko, V.V. Bel'kov, Z.D. Kvon, N.N. Mikhailov, S.A. Dvoretzkiy, D. Weiss, B. Jenichen, S.D. Ganichev. *Phys. Rev. B*, **92**, 165314 (2015).
- [7] G.M. Minkov, V.Ya. Aleshkin, O.E. Rut, A.A. Sherstobitov, A.V. Germanenko, S.A. Dvoretzkiy, N.N. Mikhailov. *Physica E*, **116**, 113742 (2020).
- [8] G.M. Minkov, V.Ya. Aleshkin, O.E. Rut, A.A. Sherstobitov, S.A. Dvoretzkiy, N.N. Mikhailov, A.V. Germanenko. *Phys. Rev. B*, **106**, 085301 (2022).
- [9] I.M. Lifshitz, A.M. Kosevich. *J. Exp. Theor. Phys.*, **2**, 636 (1956).
- [10] G.M. Minkov, O.E. Rut, A.A. Sherstobitov, S.A. Dvoretzkiy, N.N. Mikhailov, V.A. Solov'ev, M. Yu. Chernov, S.V. Ivanov, A.V. Germanenko. *Phys. Rev. B*, **101**, 245303 (2020).
- [11] C. Brüne, C. Thienel, M. Stüiber, J. Böttcher, H. Buhmann, E.G. Novik, C.-X. Liu, E.M. Hankiewicz, L.W. Molenkamp. *Phys. Rev. X*, **4**, 041045 (2014).
- [12] J. Ziegler, D.A. Kozlov, N.N. Mikhailov, S. Dvoretzkiy, D. Weiss. *Phys. Rev. Res.*, **2**, 033003 (2020).
- [13] T. Andlauer, P. Vogl. *Phys. Rev. B*, **80**, 035304 (2009).

*Translated by D.Safin*